Multi-path 2-Port Channel Characterization for Galvanic Coupled Intra-body Communication

Meenupriya Swaminathan
Electrical & Computer Engineering Department
Northeastern University
Boston, MA 02115 USA
meenu@ece.neu.edu

Joan Sebastià Pujol
Department of Electronic Engineering
Universitat Politècnica de Catalunya
Barcelona, Spain
joan.sebastia.pujol@gmail.com

Gunar Schirner
Electrical & Computer Engineering Department
Northeastern University
Boston, MA 02115 USA
schirner@ece.neu.edu

Kaushik R. Chowdhury
Electrical & Computer Engineering Department
Northeastern University
Boston, MA 02115 USA
krc@ece.neu.edu

ABSTRACT

Sensors implanted inside a body compose so called intra body networks (IBNs), which promise high degree of mobility, remote diagnostic accuracy, and the potential of directly activating the action of drug delivery actuators. To enable communication among these implanted sensors, we use the concept of galvanic coupling, in which extremely low energy electrical signals are coupled into the human body tissues by leveraging the conductive properties of the tissues. Several challenges emerge in this new communication paradigm, such as how to appropriately model the signal propagation through various tissue paths such as from muscle to skin across different tissue boundaries and quantify the achievable data rates. The main contributions in this paper are: (i) we build a 2-port tissue equivalent circuit model to characterize the body channel and to identify the range of suitable operating frequencies and (ii) we theoretically estimate the channel capacity for various sensor locations that incorporates factors like the tissue propagation path, operating frequency and noise level.

1. INTRODUCTION

Intra-body networks (IBNs) will revolutionize healthcare by allowing direct communication between implanted sensors and actuators through the body tissues. As conventional over the air radio frequency (RF) waves are strongly attenuated within the body, there is a growing concern for realizing energy-efficient transmissions within tissues. The advent of seamless, miniaturized nano-scale or MEMS-based sensors indicates possibilities for implanting several nodes that form a connected data network, apart from performing sensing and drug actuation roles. Among the candidate techniques for establishing IBNs, such as RF based, inductive coupling, capacitive coupling, and ultra-sound, we use galvanic coupling (GC). In GC-based communication, a pair of electrodes directly couple weak electric signals to the tissues in the order of 0.5 mW. The induced magnetic field is well below $2mA/m$, the permissible limit within the body [3]. Majority of the induced current coupled to the body passes through the return path of transmitter. A part of coupled signal propagates through the body and reaches the receiver electrodes (refer dashed arrow in Fig. 1(a)). The difference in voltage is detected by a corresponding pair of receiver electrodes that belong to another implant. Apart from being energy efficient when compared to RF, the communication in this scenario is less impacted by external environmental influence. In addition, GC operates with cost-effective transceivers and provides continuous real time connectivity. in terms of various network parameters. The state of the art in GC based IBNs (GC-IBN) [8, 1, 6] has been limited to on-surface communication, similar to node B to sink A communication in Fig. 1.(c). The channel behavior for implantable electrodes is obtained using a numerical model and a liquid (homogeneous) phantom reflecting typical muscle properties, but only at 27 MHz. However, to

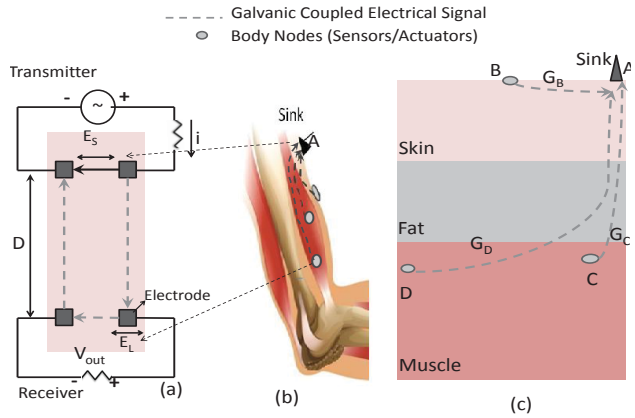

Figure 1: (a)Galvanic coupled link (b)Upper limb GC-IBN (c) Skin to skin & Muscle to skin paths

BODYNETS 2014, September 29-October 01, London, Great Britain

DOI 10.4108/icst.bodynets.2014.257023

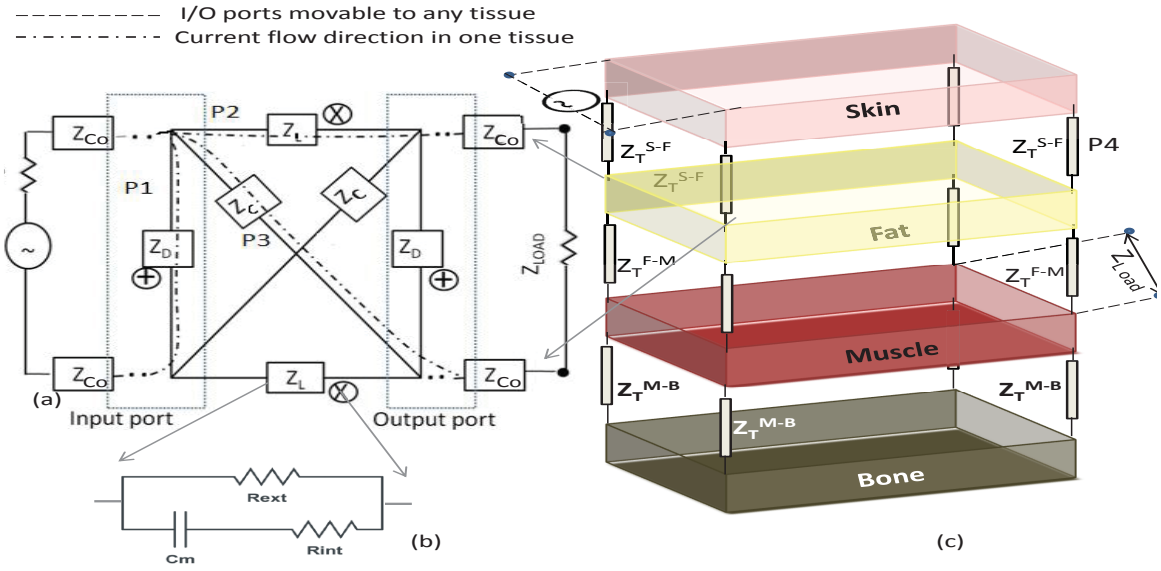

Figure 2: Equivalent circuit of (a)single tissue (b)cell, (c)electrode and coupling impedance, and (d) 2-port Model of human upper limb.

the best of our knowledge there is no work that studies the scenarios of signal propagation across tissues (Eg. from D to A in Fig. 1.(c)), demanding a three dimensional tissue structure modeling and characterizing the transverse path from one tissue to other like the one presented here. In this paper, we thoroughly explore the propagation of GC signals through various tissue paths, such as over the skin, from skin to muscle or muscle to skin and through the muscle layer, which reveal important insights on the network size, link distance and capacity of GC-IBNs. The simple transfer function derived allows quick and accurate channel modeling over a wide range of frequency. The main contributions of this paper are as follows:

1. We determine the channel gain for various tissue paths using a 2-port tissue equivalent circuit model for wireless communication through the dry skin surface and inner tissue-layers of the human arm. Our theoretical approach is validated with previously conducted experiments for on-skin cases. We provide insights on suitable implant positions inside the body tissues, operating frequency offering better channel characteristics.

2. We formulate closed form expressions for the noise that impacts correct signal reception in GC-IBN and then estimate the signal to noise ratio, which is the first step towards selection of suitable modulation schemes.

3. We then estimate the capacity of a GC link and analyze the maximum traffic that can be accommodated in GC-IBN in terms of the number of nodes.

The rest of the paper is organized as follows. We derive the 2-port equivalent circuit models of the human arm in Section 2. An approximation of possible noise in GC-IBN with SNR and capacity formulations are given in Section 3. The channel characteristics obtained using the 2-port model are discussed in Section 4, for different tissue paths, distances and frequencies. Finally, Section 5 concludes the paper.

2. 2-PORT CIRCUIT MODEL

Individual tissues are represented as *black-boxes* in a 2-port model, constructed from the electrical properties of tissues that is configurable with tissue dimensions corresponding to a specific human subject. The principle benefit of this 2-port model is a simple first-approximation for the voltages and currents that are likely to be observed within the given tissue layer during communication. The black-box approximation makes it easier to add, remove or modify tissue dimensions within the model which otherwise is complicated and time consuming to alter the model appropriately for different parts of the body. The model works for signal propagation within the same tissue layer, adapts easily for different combinations of tissues, and describes the signal propagation through tissues from the input to output ports for a given choice of input frequency, transmitter-receiver distance (D), terminal separation (E_S) (refer Fig. 1(a)) and tissue thickness (T). As an added advantage, the port parameters enable direct observation of the scattering parameters at the electrode-tissue and tissue-tissue boundaries to assess the reflection and propagation at interfaces.

Tissue Impedance: When live tissue cells are excited by an electrical signal, each cell activates its neighbor, enabling signal propagation through different paths. The cell membrane gives a capacitance effect allowing only the high frequency signal to pass through while the low frequency signal takes the extra-cellular path. Therefore, a biological cell can be modeled as parallel combination of resistance R_{ext} (dissipation loss), and a combination of capacitor C_m and intra-cellular resistance R_{int}, as given in Fig. 2(b). The R and C values can be completely described in terms of conductivity (σ) and relative permittivity (ϵ) using Cole-Cole model [2]. The tissue admittance using RC elements can be calculated as,

$$Y = F_W \left(\sigma M_1 + \frac{1}{\sigma \kappa M_1 + j\omega \epsilon M_2} \right) \quad (1)$$

where M_1 is the ratio of cross sectional area (A) and length of the channel (L) decided by the direction of impedance measurement, while M_2 is the ratio of A and thickness of channel, $F_W \in [1, 10]$ is the correction factor accounting for variation in tissue water distributions. κ is the ratio of external to internal cell resistance. The tissue properties can be estimated without actual measurement such as tissue thickness approximation using BMI or triceps skin fold thickness.

Single Tissue Equivalent Circuit: The 2-port equivalent of a single GC-coupled tissue is modeled using tissue impedance along the four propagation paths P1, P2, P3 (Fig. 2(a)) and P4 (Fig. 2(c)) taken by the injected current that are obtained as follows.

- P1 is the primary return path offering the direct impedance Z_D that channels the majority of current from the terminal to reference electrodes in the transmitter. In this case M_1 given in (1) takes the form $(E_L \times T)/E_S$, where E_L is a side of the square electrode, T is tissue thickness and E_S is the terminal-reference electrodes separation in transmitter/receiver.

- P2 serves as a pathway for a portion of current directed towards the receiver electrodes through longitudinal impedance Z_L, between the transmitter and receiver electrodes. M_1 of Z_L is calculated as $(E_L \times T)/D$, where, D is the transmitter-receiver separation distance.

- P3 is the current propagation path from source terminal in transmitter to the reference terminal in receiver through cross impedance Z_C. Here, M_1 becomes $(\sqrt{2}E_L \times T)/(\sqrt{D^2 + E_{ST}^2})$. In all the above cases, M_2 is chosen to be the tissue thickness.

- P4 is the current propagation path to adjacent tissue layer through transverse impedance Z_T. To compute this impedance, M_1 is substituted with T/A_e, where, A_e is the electrode area. In this case, M_2 is assigned the value of E_S.

The coupling impedance offered by the electrode-tissue interface determines the amount of signal entering into the tissue. This impedance, denoted as Z_{Co} (refer Fig. 2(a)), is a function of frequency, area of contact, tissue hydration, electrode material and surface treatment and is modeled similar to the approach in [5] as

$$R_{Co} = \rho_{Co} f^m / A_e \text{ and}$$

$$X_{Co} = 1/wC_{Co} = K_1 \epsilon_{Co} f^m / A_e$$

where, f is the frequency of operation, ρ_{Co} is the electrode and hydrogel resistivity, A_e is electrode area, $K_1 \in (0, 1)$ is chosen based on the tissue hydration, ϵ_{Co} depends on electrode permittivity, and m is the constant for activation control. The dots in Fig.2(a) represents the possibility of attaching Z_{Co} to any tissue based on the tissue path under study. For instance, in the skin to muscle path, the coupling impedance is included in input impedance of skin and output impedance of muscle. Using the impedance defined above, the 2-port equivalent of a tissue can be defined in terms of Z-parameters represented as a 2×2 matrix of complex numbers that obeys the relation, $[V] = [Z]\,[I]$ where $[V]' = [V_1\ V_2]$ is the voltage vector, and $[I]' = [I_1\ I_2]$ is the current vector at the input and output ports. The Z parameter of each tissue can be calculated as,

$$[Z] = \begin{bmatrix} Z_{11} & Z_{12} \\ Z_{21} & Z_{22} \end{bmatrix} = \begin{bmatrix} \frac{2Z_1Z_2}{Z_1+2Z_2} & \frac{Z_1Z_2}{Z_1+2Z_2} \\ \frac{Z_1Z_2}{Z_1+2Z_2} & \frac{Z_1Z_2+Z_2^2}{Z_1+2Z_2} \end{bmatrix}$$

with $Z_1 = \left(\frac{2Z_LZ_T}{Z_T - Z_L}\right)$ and $Z_2 = \left(\frac{Z_TZ_D}{Z_T+Z_D}\right)$. For the tissue layer receiving signal from another layer, Z_1 becomes $\left(\frac{2Z_LZ_T}{Z_T-Z_L}(1+Z_T)\right)$, where Z_T is the transverse impedance offered by the interface between tissue layers. Similar to impedance parameters, we also use admittance parameters $[Y]$ for handling parallel impedance and ABCD parameters $[A]$ for handling cascaded impedance.

2.1 Human Arm Equivalent 2-port Network

We approximate the galvanic coupled human arm as layered dielectric block of tissues as given in Fig. 2.(c). The model of 700 mm length has four tissue layers - outer dry skin, fat, muscle and cortical bone (hard outer covering of bone) of thickness 1 mm, 9 mm, 25 mm and 20 mm respectively. For developing a tractable model, we assume uniform tissue dimensions along the paths indicated by $\bigoplus$ and $\bigotimes$ in Fig. 2(a). However, it is possible to introduce asymmetry in the model by varying the electrodes separation E_S, and/or T at transmitter and receiver.

In the following multi-layer discussion the superscript i and j denote a specific tissue layer, i.e., $i, j \in \{S, F, M, B\}$, with the substitutions of S for skin, F for fat, M for muscle, and B for bone. The single tissue impedance Z_D and Z_L in Fig. 2.(a) become Z_D^{i-i} and Z_L^{i-i} and Z_T takes the form Z_T^{i-j}, denoting path from layer i to j. The transmitter electrodes, attached on the tissue, form the input port, and the receiver electrodes form the output port. This concept is clarified further with a sample case of the transmitter and receiver coupling locations on skin to muscle path (S-M path) is shown in Fig. 2.(c). Figure 3 illustrates the location of coupling electrodes when on-surface nodes are moved into muscle tissue. We explain the development of the analytical models for skin to skin (S-S), muscle to muscle (M-M), skin to muscle (S-M) and muscle to skin (M-S) tissue paths of signal propagation next. We ignore the paths through fat and bone tissues as the implants are not commonly placed in these tissues.

• ***S-S path model*** Here, the transmitter and receiver sensor electrodes are positioned on the skin surface with coupling impedance Z_{Co}. The current flow is through skin, and through the parallel paths in fat, muscle and bone layers. The input impedance of the fat layer includes the transverse impedance from skin as the signal originates in skin. Similarly, the input impedance of muscle and bone layers include the transverse impedance from the fat and muscle tissues, respectively. The overall admittance is:

$$[Y^{S-S}] = [Y^S] + [Y^F] + [Y^M] + [Y^B] \quad (2)$$

• ***M-M path model*** To study the channel response at the muscle layer, the transmitter and receiver sensor electrodes are moved inside muscle tissue (M-M path), in which the dominant path of the current also lies. Along the M-M path, the muscle tissue is in parallel to that of skin and fat tissues

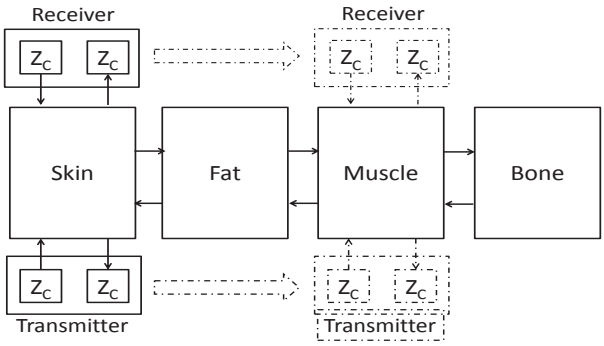

Figure 3: Coupling impedance location for transmitter and receiver moving from on-skin to muscle

and with the bone. In this case, the input impedance of fat and bone layers include the transverse impedance from the muscle layer as the signal originates from the muscle. The input impedance of skin layer includes the transverse impedance of muscle and fat tissues. The total channel admittance at M-M path can be calculated as the parallel combination of individual tissues as given in S-S path model.

• ***S-M path model*** When the transmitter is on skin and the receiver is in muscle, the impedance offered by the S-M path is measured as the cascaded skin-fat-muscle ports that is in parallel to that of bone. The transverse impedance is calculated as in the S-S case as the signal source is at skin. Assuming A^S, A^F and A^M as the $[A]$ parameters of skin, fat and muscle, the combined $[A]$ parameter for the cascaded skin-fat-muscle tissues is given by

$$[A^{S,F,M}] = [A^S].[A^F].[A^M] \tag{3}$$

With the added parallel effect of bone tissue, the overall admittance of the S-M path is computed as follows.

$$[Y^{S-M}] = \begin{bmatrix} \frac{A_{22}^{S,F,M}}{A_{12}^{S,F,M}} & \frac{-\triangle[A^{S,F,M}]}{A_{12}^{S,F,M}} \\ \frac{-1}{A_{12}^{S,F,M}} & \frac{A_{11}^{S,F,M}}{A_{12}^{S,F,M}} \end{bmatrix} + [Y^B] \tag{4}$$

• ***M-S path model*** For the M-S path, with the source at muscle, the transverse impedance is calculated as in M-M path. Here, the ABCD parameter of cascaded muscle, fat and skin tissues is given by

$$[A^{M,F,S}] = [A^M].[A^F].[A^S] \tag{5}$$

The admittance parameter of M-S path is obtained by computing the cascaded muscle, fat and skin tissue in parallel to the bone. The resulting expression is similar to the computation in (4). The voltage gain $G(w, E_L, D, E_S, [T])$ can be calculated from the total equivalent Z parameters (inverse of Y parameter matrix) $[Z^{i-j}]$ as,

$$\frac{V_{out}}{V_{in}} = \frac{Z_{21}^{i-j} Z_{Load}}{(Z_{11}^{i-j} + Z_{Co})(Z_{22}^{i-j} + Z_{Load}) - Z_{12}^{i-j} Z_{21}^{i-j}} \tag{6}$$

where $i, j \in \{S, M\}$ for denoting S-S, S-M, M-S and M-M paths individually. The gains along the four paths above is plotted in Fig. 5 and analyzed in section 4.

3. NOISE, SNR & CAPACITY ESTIMATION

To fully determine the ability of the receiver to decode the signal and determine the achievable data rate, the estimation of noise is of critical importance. Once this noise level is known, the signal to noise ratio (SNR) can be computed, and the impact of various modulation schemes can be studied. To quantify the noise level, we focus on a single pair of transmitter-receiver nodes. We model the noise by approximating the power spectral densities (p.s.d) of thermal noise, electrode coupling noise and RF radiation interference as described below.

Thermal Noise N_T: The thermal noise depends mainly on frequency and temperature can be calculated as:

$$N_T(f) = \sqrt{4KTR} \;\; W/\sqrt{Hz} \tag{7}$$

where T is the absolute temperature in Kelvin, K is Boltzmann constant, and R is electrode and tissue resistance.

Electrode coupling noise $N_E(f)$: This noise occurs at the interface where the electrode is attached to the tissue. The skin-electrode interface noise can be related to the real part of the skin-electrode impedance, and is equivalent to the thermal noise at high frequencies. We use the noise p.s.d of surface electrodes as approximated in [4] as:

$$N_E(f) = 1/f^{\alpha}, \;\; 1.5 < \alpha < 2.0 \tag{8}$$

where α is a correction factor that depends on the gel type and skin properties.

RF Radiation interference I_o: RF radiation from sources including TV and radio broadcast signals, transmissions in the so called *lost band* $(160 - 190$ KHz) and amateur radio $(135.7 - 137.8$ KHz) that are in 100 KHz to 1 MHz range might be a potential source of interference. We approximate these interference sources as Additive White Gaussian Noise with IID Gaussian random variable $N(0, \varphi)$ of zero-mean and variance φ.

The channel's Signal to Noise Ratio (SNR) can be calculated as

$$SNR^{i-j} = \frac{P_t \cdot G^{i-j}(w, E_L, D, E_S, [T])}{(N_T + N_E + I_o).\triangle f}, \tag{9}$$

where P_t is the transmitter power and $\triangle f$ is the receiver bandwidth. The SNR estimated can be used to calculate bit error rate (BER) for a given modulation type, f and D. We term the maximum distance of communication between the transmitter and receiver beyond which the BER exceeds the desired value as the threshold distance D_{Th}. For a node to communicate with sink at a distance $D > D_{Th}$, (say from

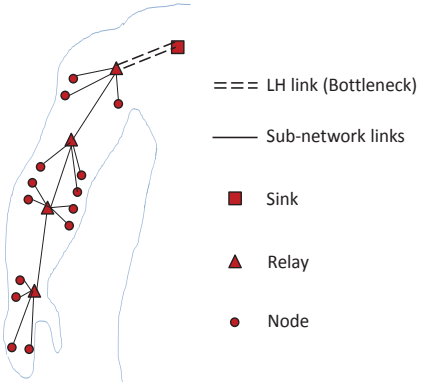

Figure 4: GC-IBN topology at human arm

Table 1: Gain, Capacity and BER for BPSK Modulation at $\varphi = 1e8$

Distance (cm)	Frequency (KHz)	Gain (dB)			Channel Capacity (bps)			BER (BPSK)		
		S-S	M-S	M-M	S-S	M-S	M-M	S-S	M-S	M-M
10	100	-37	-30.5	-18	3.70E+05	5.80E+05	9.90E+05	10^{-7}	10^{-28}	10^{-50}
10	1000	-38	-38.5	-16.8	3.40E+05	3.30E+05	1.03E+06	10^{-5}	$10^{-4.5}$	10^{-52}
20	100	-52	-47	-31	4.00E+04	1.20E+05	5.70E+05	$10^{-1.5}$	10^{-2}	10^{-27}
20	1000	-53	-55	-29.7	4.00E+04	2.60E+04	6.10E+05	10^{-1}	$10^{0.8}$	10^{-30}

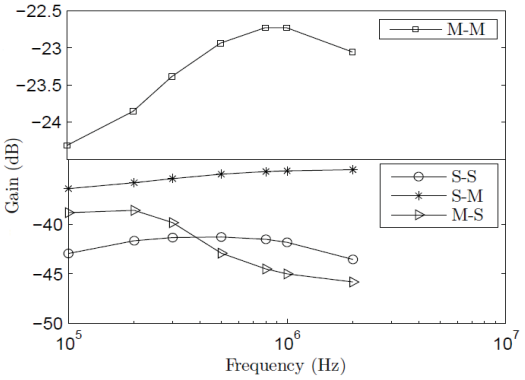

Figure 5: (a)Gain at 4 paths (D=15cm, $E_L = 1cm$, & $E_S = 5cm$)

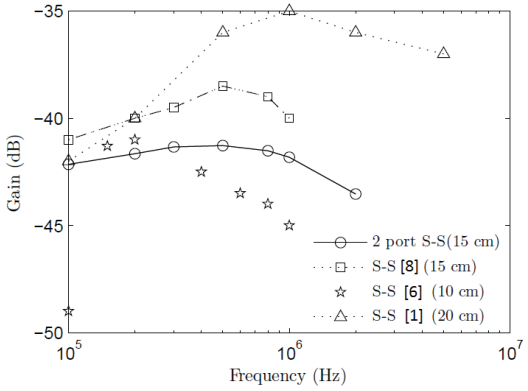

Figure 6: S-S path gain comparison from literature.

a node implanted at wrist to sink on shoulder), multi-hop paths using relays are required. We assume that a relay could connect a number of nodes in single hop arranged in a star topology. Each relay in-turn could be connected to the sink via multi-hop links. When a spanning tree is constructed that connects all the nodes in an upper limb to a sink through relays as illustrated in Fig.4, it results in the formation of a bottleneck link. This link carries the entire upper limb traffic to the sink that we call as the last hop link (LH), (refer Fig.4). The capacity of LH link, C(LH), for various lengths and paths of LH using Shannon - Hartley theorem, can be determined as

$$C(LH) = W\ log_2(1 + SNR^{i-j})\ [bits/s], \forall i, j \in \{S, M\}$$

where W is transmission bandwidth. According to Max-flow Min-cut theorem, a minimum cut on LH, with maximum capacity C(LH), limits the maximum number of nodes in the sub-network and the maximum possible data rate at each node [7].

For reliable communication to and from the upper limb GC-IBN, the total traffic through LH should be less than C(LH). Consequently, for the N nodes in upper limb sub-tree to communicate reliably, the following condition has to be satisfied.

$$\sum_u R(u) < C(LH), \forall u \in \{1, ..., N\} \tag{10}$$

where R(u) is the total data rate to and from node u. Assuming equal data rate $\hat{R}$ in all the N nodes, the maximum possible N in subnetwork, N_{Max} is limited by

$$N_{Max} < \frac{C(LH)}{\hat{R}} \tag{11}$$

.

4. RESULTS AND DISCUSSIONS

The channel gain obtained for the four paths obtained using the 2-port model derived in Sec.2 at $D = 15$cm, $E_S = 5$cm, and $E_L = 1$cm are given in Fig. 5. The gain along the S-S path has a peak at 500 KHz and decreases beyond 1MHz.

• ***Results verification using literature:*** The clinical trial results in [8] match exactly with our analytical results as the measurement set-up is similar to our model assumptions presented above. However, though our results matches closely with the other literature measurement at 100 KHz as shown in Fig.6, there is a difference of approximately 7 dB and 3 dB with [1] and [6] respectively at 1 MHz.

The difference in gain in the latter two cases are likely due to the variations in the electrode dimensions, electrode material, physical tissue dimensions in the measurement set-ups. For instance, in [6], the skin thickness was assumed to be 1.5 mm with $E_S = 80$ mm while we assigned them 1 mm and 100 mm respectively. Similarly, in [1], the radius of the subject's arm is 47.5 mm, which we modeled as 55 mm. There are other inherent measurement uncertainties including surface treatment at electrode attachment, tissue temperature and hydration levels that we model using parameters F_W and Z_{Co} and are not specified in the corresponding literature. Also, the conductivity and permittivity of tissues also vary among individuals by +/- 0.1 S/m and +/- 0.05 S/m in the range of frequency used [9] that contribute to the difference between our results and the results in [1] and [6]. In order to overcome other measurement uncertainties in GC-IBN, an adaptive communication system is required that alters the transmission parameters based on the time de-

pendent estimation of channel characteristics. For instance, estimating bounds on interference and allowing sufficient tolerance levels in transmission power control schemes would help alleviating the above mentioned uncertainty.

• ***Tissue paths comparison:*** Among the four paths, M-M path has the largest gain of -24.5 to -22.5 dB be due to the higher conductivity and larger volume of muscle. The gain is increasing with frequency upto 800 KHz and falls low at higher frequencies. The higher gain in M-M path is also caused by the signal trapping in inner tissues with little dissipation to air. In the S-S path, however, owing to the immediate coupling with surrounding air, the maximum gain is only around -41 dB at 500 KHz. The lower values of dry skin conductivity and thickness also leads to higher attenuation in S-S path. The channel gain can be improved by using suitable surface treatments such as application of conductive gels at the electrode attachment location.

The signal originating on-skin primarily propagates through low resistant muscle. Therefore, with a source on skin, a receiver in muscle (S-M path) experiences better channel gain compared with an on-skin receiver (S-S path). The loss of S-M path being $\approx$ 10 dB more than the M-M path is due to the initial loss at the skin tissue and the intermediate fat tissue with Z_T^{S-F} and Z_T^{F-M}. Along the M-S path, the gain is high (-38.5 dB) at 200 kHz and decreases with frequency (to -46 dB) indicating higher gain than S-S path at frequencies lower than 200 kHz. At higher frequencies, M-S path offers the worst gain among all the paths. Hence, surface to implant communication through S-M path offers significant benefit at higher frequency while implant to on-surface communication performs better at lower frequency. At frequencies higher than 1 MHz, majority of the signal leaks from the tissue to the surrounding space that cannot be received by body nodes. For this reason, we avoid the frequencies above 1 MHz and also the frequencies below 100 kHz that may comprise the body's natural frequencies.

• ***BER & link capacity:*** Assuming a bandwidth of 100 kHz and 1 MHz, with input power of 1 mW, φ of $1e8$ and SNR estimated using (9), the BER calculated for BPSK modulation technique is given in Table.1 for 10 cm and 20 cm between the transmitter and receiver. The M-M path offers minimum BER for both 10 cm and 20 cm. On the other hand, a maximum BER of greater than unity is offered by the M-S path with $D = 20$ cm operating at 1 MHz. However, the same M-S path gives reliable communication with BER $<10^{-4}$ at both frequencies with $D = 10$ cm, which is similar to the S-S path. The S-M path performs better than S-S and M-S paths in terms of BER for the distances and frequencies considered in this analysis. At $D = 10$ cm, the maximum capacity of 1.03 Mbps is achieved in M-M path with $f = 1$ MHz. At $D = 20$ cm, M-S path offers a minimum capacity of 26 kbps.

• ***Threshold distance & N_{Max}:*** If communication is assumed to be reliable when BER $<10^{-4}$, at 100 kHz S-S path gives better gain upto 13 cm. The D_{Th} attainable along M-S, S-M and M-M paths are 19 cm, 24 cm and 32 cm respectively. Using (10), (11), D_{Th} and capacity of GC-IBN links, we estimated N_{Max} for BPSK modulation, at 100 kHz, φ =$1e7$ and $1e8$, with R=100 & 10,000 bps and the results are given in Table.2. According to the results, at $\varphi = 1e7$, and $D = 20$ cm, S-S path could connect only one node in the subnetwork with $R = 10$ Kbps. However, there could be upto nearly 10,000 nodes in subnetwork on M-M path with $\varphi = 1e8$, $D = 10$ cm, each with R=100 bps.

Table 2: N_{Max} at 100 KHz

φ	$\hat{R}$	D(LH)=10 cm			D(LH)=20 cm		
	(Kbps)	S-S	M-S	M-M	S-S	M-S	M-M
1e7	0.1	2283	4191	8267	166	471	4035
	10	22	41	82	1	4	40
1e8	0.1	3720	5790	9981	487	1210	5685
	10	37	57	99	4	12	56

5. CONCLUSIONS

The channel gain calculations, the achievable range of communication, BER and link capacities analyzed in this paper demonstrates GC-IBN as a feasible candidate for network implanted body nodes. Our 2-port model helps in quick characterization of the channel within the body. We have derived the expressions for noise and data rates that are feasible in such networks and future work will be focused on higher layer networking design.

6. ACKNOWLEDGEMENTS

This material is based on the work supported by the U.S. National Science Foundation under grants CNS-1136027 & CNS-1453384.

7. REFERENCES

[1] M. Amparo Callejon, D. Naranjo-Hernández, J. Reina-Tosina, and L. M. Roa. Distributed circuit modeling of galvanic and capacitive coupling for intrabody communication. *IEEE Trans. on Biomedical Engineering,*, 59(11):3263–3269, 2012.

[2] D. Miklavčič, N. Pavšelj, and F. X. Hart. Electric properties of tissues. *Wiley encyclopedia of biomedical engineering*, 2006.

[3] Guidelines for limiting exposure to time-varying electric, magnetic, and electromagnetic fields (up to 300 ghz). *Health Phys*, 74(4):494–522, 1998.

[4] E. Huigen, A. Peper, and C. Grimbergen. Investigation into the origin of the noise of surface electrodes. *Medical and biological engineering and computing*, 40(3):332–338, 2002.

[5] H. Kanai, I. Chatterjee, and O. P. Gandhi. Human body impedance for electromagnetic hazard analysis in the vlf to mf band. *IEEE Trans. on Microwave Theory and Techniques*, 32(8):763–772, 1984.

[6] Y. Song et al. The simulation method of the galvanic coupling intrabody communication with different signal transmission paths. *IEEE Trans. on Instrumentation and Measurement*, 60(4):1257–1266, 2011.

[7] M. Stoer and F. Wagner. A simple min-cut algorithm. *Journal of the ACM (JACM)*, 44(4):585–591, 1997.

[8] M. S. Wegmueller et al. Signal transmission by galvanic coupling through the human body. *IEEE Trans. on Instrumentation and Measurement*, 59(4):963–969, 2010.

[9] C. Gabriel et al. Electrical conductivity of tissue at frequencies below 1 MHz. *Physics in medicine and biology*, 54(16): 4863, 2009.